Redshifted 21 cm Emission From the Pre-Reionization Era
I. Mean Signal and Linear Fluctuations

Nickolay Y. Gnedin

CASA, University of Colorado, Boulder, CO 80309, USA; gnedin@casa.colorado.edu

and

Peter A. Shaver

ESO, Karl-Schwarzschild-Strasse 2, Garching, D-85748, Germany; pshaver@eso.org

ABSTRACT

We use cosmological simulations of reionization to predict the possible signal from the redshifted 21 cm line of neutral hydrogen in the pre-reionization era and to investigate the observability of this signal. We show that the separation of the mean (global) signal over the whole sky from the known foreground contamination may be feasible, but very challenging. In agreement with previous studies, we demonstrate that measuring angular fluctuations in the H I signal is likely to be extremely difficult if not impossible because of the overwhelming contamination from the galactic and extragalactic foregrounds. However, we show that the sharp H I fluctuations in the frequency domain should be easily separable from the relatively smooth spectra of the foregrounds, and that these fluctuations should be detectable even at moderate angular resolution ($\sim 10 - 20$ arcmin).

Subject headings: cosmology: theory - cosmology: large-scale structure of universe - diffuse radiation - galaxies: formation - galaxies: intergalactic medium - radio lines: general

1. Introduction

The importance of the 21 cm line of neutral hydrogen has long been recognized for its potential in studying the reionization of the universe. This possibility has been emphasized many times in a large volume of previous research, beginning with the pioneering work of Sunyaev & Zel'dovich (1972), through the first application of this idea to the modern scenario of galaxy formation by Scott & Rees (1990), to the recent detailed investigations (Madau, Meiksin, & Rees 1997; Gnedin & Ostriker 1997; Shaver et al. 1999; Tozzi et al. 2000; Di Matteo et al. 2002; Iliev et al. 2002; Ciardi & Madau 2003; Iliev et al. 2003; Furlanetto, Sokasian, & Hernquist 2004; Oh & Mack 2004, Zaldarriaga, Furlanetto, & Hernquist 2004).

The shape and strength of the 21 cm signal is ultimately connected to the process of reionization of the universe. As numerical simulations of reionization (Gnedin 2000; Ciardi, Stoehr, White 2003; Sokasian et al. 2003; Ciardi, Ferrara, & White 2003) become more detailed and precise, it becomes possible to construct detailed reionization histories of the universe that are consistent with recent observational data such as the Lyman-alpha flux decrement in the IGM up to $z \sim 6$, and which, therefore, can be used to make quantitative predictions about the expected 21 cm signal.

The difficulty of measuring the 21 cm signal is not so much its weakness as the overwhelming contamination from galactic and extragalactic foregrounds (Shaver et al. 1999; Di Matteo et al. 2002; Oh & Mack 2004) at these frequencies ($\nu \sim 100 - 200$ MHz). So the question of the observability of the signal - which includes both the mean signal over the whole sky and fluctuations in both the angular and frequency domains - is

the question of separating the cosmological signal from the foreground contamination.

In this paper we consider the widespread fluctuations in the 21 cm signal caused by the (linear) density fluctuations in the cosmic gas. Additional fluctuations in the 21 cm signal can also appear in special regions, such as individual H II regions around possible rare bright high redshift quasars (Madau et al. 1997); this topic will be the subject of a forthcoming paper. But even if the signal from the vicinities of high redshift quasars is more easily measurable, observations of quasars do not substitute for the search for linear density fluctuations. Observing signatures of quasars in the redshifted 21 cm signal will tell us important information about the very first AGNs in the universe, but they will not provide the kind of information that can be extracted from the measurement of linear fluctuations.

For example, measuring the amplitude of the linear density fluctuations at $z \sim 10$ provides information about the evolution of the matter power spectrum at redshifts intermediate between those probed by the CMB ($z \sim 1000$) and those probed by galaxy surveys ($z \sim 1$). Such information will be important in placing complimentary constraints on cosmological parameters and the evolution of the cosmic equation of state.

2. Simulations

Since our goal is to investigate the observability of the redshifted 21 cm line from the early universe, we need a plausible model for the evolution of the physical state of the cosmic gas at that epoch. We use numerical simulations with the Softened Lagrangian Hydrodynamics (SLH) code similar to those reported in Gnedin (2000). The advantage of using the SLH code is that it incorporates all of the important physical processes that affect the reionization of the universe and the emission and absorption in the 21 cm line:

Dark matter is followed using the adaptive Particle-Particle-Particle-Mesh (P^3M) algorithm (Gnedin & Bertschinger 1996).

Gas dynamics is followed on a quasi-Lagrangian deformable mesh using the SLH algorithm.

Star formation is included using the Schmidt law in resolution elements that sink below the numerical resolution of the code.

Ionization and thermal balance of the hydrogen and helium plasma are followed exactly using a two-level implicit scheme.

Molecular hydrogen formation and destruction are followed exactly (including radiative transfer effects) in the limit when the fraction of hydrogen in the molecular form is small and the self-shielding of H_2 is unimportant. (The latter is always the case in the simulation presented in this paper because the numerical resolution is not sufficient to resolve the formation of molecular clouds.)

Radiative transfer is treated self-consistently in a 3D spatially-inhomogeneous and time-dependent manner using the Optically Thin Variable Eddington Tensor (OTVET) approximation of Gnedin & Abel (2001).

The SLH code also incorporates two important physical effects that were emphasized by Madau, Meiksin, & Rees (1997): heating by X-ray halos around galaxies and heating by secondary electrons. The first effect is included automatically by virtue of using the gas dynamical simulation, while the second effect is incorporated explicitly in the code as explained in (Ricotti, Gnedin & Shull 2003).

Our knowledge of the evolution of the early universe is sketchy at best. Therefore, in order to cover a sufficient parameter space, both in terms of the cosmological parameters and possible variations in the relative importance of different physical processes, we have run several different sets of cosmological simulations.

Star formation is incorporated in the simulations using a phenomenological Schmidt law, which introduces two free parameters: the star formation efficiency ϵ_{SF} (as defined by eq. [1] of Gnedin 2000) and the ionizing radiation efficiency ϵ_{UV} (defined as the energy in ionizing photons per unit of the rest energy of stellar particles).

Each set of simulations includes several runs with different values of these parameters, and two pieces of observational data are used to constrain the parameters. The star formation efficiency ϵ_{SF} is chosen so as to normalize the global star for-

mation rate in the simulation at $z = 4$ to the observed value from Steidel et al. (2001), and the ultraviolet radiation efficiency ϵ_{UV} is constrained by the condition that the simulation reproduces the mean transmitted flux in the Lyman-alpha forest at $z \approx 6$ as measured by White et al. (2003).

Parameters of the four sets of simulations that we use in this paper are given in Table 1. All simulations include 128^3 dark matter particles, an equal number of baryonic cells on a quasi-Lagrangian moving mesh, and about 3 million stellar particles that form continuously during the simulation[1], with the exception of the set D, in which only 64^3 dark matter particles and baryonic cells are used - the latter set includes several simulations with varied physical modeling, as explained below, which makes it impractical to include a larger number of resolution elements. The nominal spatial resolution of simulations is fixed at $1h^{-1}$ comoving kpc, with the real resolution being a factor of two lower.

In all cases a flat cosmology is assumed, with $\Omega_{\Lambda,0} = 1 - \Omega_{m,0}$, and normalization of the primordial fluctuations is determined either from the *WMAP* data (Spergel et al. 2003) for set A, or from the *COBE* data (White & Bunn 1995) for the other three sets.

Given a simulation, we calculate the relative populations of hyperfine levels of neutral hydrogen, taking into account the effects that determine the level populations at high redshift: Lyman-alpha pumping and collisions with both electrons and hydrogen atoms (Tozzi et al. 2000). We then generate synthetic spectra at different points on the simulated sky, and average them appropriately (depending on the observation modeled), which provides us with the most accurate computation of the emission signal, including velocity focusing.

---

[1]Stellar particles sample the phase space density of the stellar component; they do *not* represent individual stars or star clusters.

Table 1: Simulation Parameters

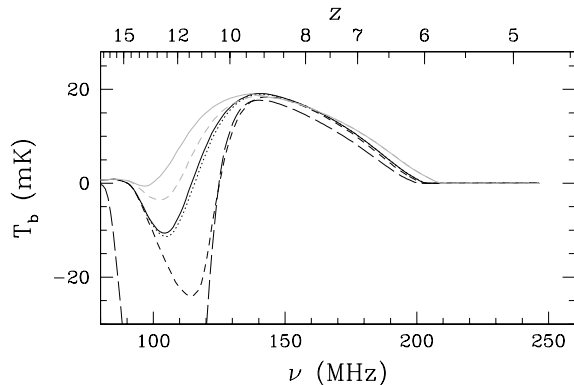| Set	Ω_m	h	n	Box size	Resolution
A	0.27	0.71	1.0	$4h^{-1}$ Mpc	$1h^{-1}$ kpc
B	0.35	0.70	0.95	$4h^{-1}$ Mpc	$1h^{-1}$ kpc
C	0.35	0.70	0.97	$4h^{-1}$ Mpc	$1h^{-1}$ kpc
D	0.35	0.70	0.95	$2h^{-1}$ Mpc	$1h^{-1}$ kpc

Fig. 1.— The mean (over the whole sky) excess brightness temperature as a function of frequency and redshift for several simulations from set D: the fiducial model (black solid line), the same model with no heating by Lyman-alpha recoil (black dotted line), with no Lyman-alpha heating and no radiation above 4Ry (black short-dashed line), and with no Lyman-alpha heating, no radiation above 4Ry, and no shock heating (black long-dashed line). Two gray lines show the fiducial model with sources of ionization having a power-law quasar-like spectrum rather than a stellar-type spectrum. The solid gray line shows the model without secondary electrons included, while the gray dashed line shows the same model with secondary electrons included. All models are normalized to fit the observed evolution of the mean transmitted flux in hydrogen Lyamn-alpha line, as explained above.

It is interesting to look at the physical effects that might control the characteristics of the redshifted 21 cm emission. Simulations are the ideal tool to make such a study, because they offer complete control over their physical ingredients, as is demonstrated in Figure 1.

Our fiducial model includes all relevant physical effects, and assumes that sources of ionization have a stellar spectrum (see Gnedin 2000 for details). The prediction of the fiducial simulation from set D that best fits the mean transmitted Lyman-alpha flux data at $z \sim 6$ for the mean (averaged over the whole sky) 21 cm signal is shown in Figure 1 with a black solid line.

There are several features in this curve. The curve starts to deviate from zero at $z \sim 15$ - this is the moment when the first sources of Lyman-alpha radiation begin to form in the simulation. The Lyman-alpha photons couple the level population of the hyperfine transition in neutral hydrogen to the kinetic temperature of the gas (c.f. Tozzi et al. 2000) and drive them out of equilibrium with the Cosmic Microwave Background (CMB). Because initially most of the gas in the universe is colder than the CMB, the signal is seen as absorption against the CMB. By $z \sim 12$, the mean gas temperature has however risen above the CMB temperature (the specific source of this heating is discussed in the following paragraphs), so the 21 cm signal switches from absorption to emission. At $z \sim 10$ the ionization fronts in our fiducial model start to expand in the low density IGM, which occupies most of the volume of the universe and at $z \sim 10$ still contains most of the mass. This process results in a progressively larger fraction of neutral hydrogen being ionized and a progressively lower 21 cm signal, until, finally, the universe is fully reionized by $z \sim 6$ (in accord with the SDSS observations, White et al. 2003), and the 21 cm signal becomes unmeasurably small.

The characteristic transition from absorption to emission at $z \sim 11 - 12$ is controlled by the heating of the cosmic gas. What is the primary source of gas heating? Using the simulations from the set D, we have investigated the role of various physical effects on the shape of the cosmological 21 cm signal. The advantage of using simulations is that we can switch various physical effects on and off at will. For example, the dotted line in Fig. 1 shows the brightness temperature evolution for the simulation, in which we do not include the heating by recoil of Lyman-alpha photons in the temperature equation for the cosmic gas. As one can see, the effect of Lyman-alpha recoil is not significant in our fiducial model. This conclusion fully agrees with Chen & Miralda-Escudé (2003).

In the further exploration of importance of various physical effects, we show with the short-dashed line in Fig. 1 out fiducial model, but with both Lyman-alpha heating and heating by X-rays excluded. i.e. all sources are assumed to emit no radiation above 4 Ry. As can be seen, X-rays have a substantial effect on the evolution of the excess brightness temperature at $15 > z > 9$ (in this particular cosmological model). Thus, early X-rays play a major role in the evolution of the IGM temperature, as has been emphasized earlier by Madau et al. (1997), Tozzi et al. (2000), and Chen & Miralda-Escudé (2003).

In the third simulation we have excluded the shock heating as well (in addition to Lyman-alpha heating and X-ray heating). In other words, we only allowed photoionization heating as the single source of heating of the gas in that simulation. The result of that simulation is shown as a long-dashed line in Fig. 1. This change makes a dramatic difference - most of the gas heating at high redshifts is due to shocks (i.e. structure formation). However, the cosmological parameters are thought to be sufficiently well known (Tegmark et al. 2004) that uncertainties in the shock heating rate are not dominant.

To further illustrate the role of X-rays in controlling the 21 cm emission at high redshifts, we show with the solid grey line a simulation in which all sources of ionization have a hard, quasar-like spectrum, rather than a stellar spectrum as in the fiducial model. In that case there is almost no stage in which the the redshifted 21 cm line appears in absorption, because the gas heating is extremely efficient. Finally, the dashed grey line shows the same model with secondary electrons included. The conclusion we draw from Fig. 1 is that the details of the early absorption phase in the 21 cm emission and the transition from absorption to emission depend on details of the early universe physics, and, therefore, can be used as a powerful test of the first episode of galaxy formation. On the other hand, the observed evolution of the mean transmitted flux in the hydrogen Lyman-alpha line (White et al. 2003) strongly constrains the late stages of the reionization process and the predicted 21 cm emission for redshifts less than about 9. In the rest of this paper, we focus on this late reionization stage when we need a robust estimate of the cosmological 21 cm signal.

Finally, in a further exploration of various physical effects responsible for the redshifted 21 cm emission, we show in Figure 2, at the request of the referee, evolution of the mass-weighted average coupling efficiency y, which is defined via the following equation:

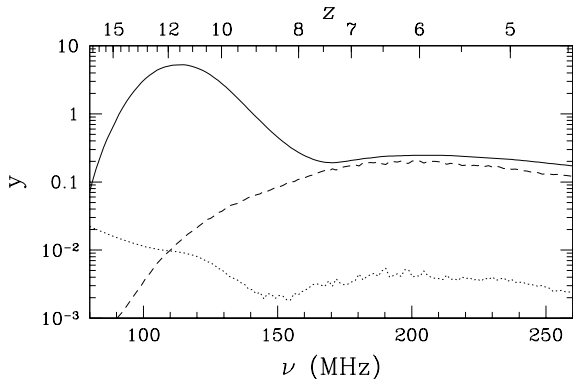$$T_S = \frac{T_{\text{CMB}} + yT_K}{1 + y}, \qquad (1)$$

4

Fig. 2.— The evolution of the mass-weighted average efficiency y of coupling between the gas kinetic temperature and the spin temperate of the 21 cm line in the fiducial model A for three main coupling mechanism: Lyman-α pumping (solid line), collisions with neutral atoms (dotted line), and collisions with free electrons (dashed line).

where T_K is the gas kinetic temperature, and T_S is the spin temperature of the redshifted 21 cm line. Three independent physical processes make contributions to y: pumping by Lyman-α photons, and collisions with neutral atoms and free electrons (Madau et al. 1997; Tozzi et al. 2000), which are shown with different lines in Fig. 2. As one can see, the Lyman-α pumping dominates over the other two mechanisms for $z \gtrsim 8$, in agreement with Madau et al. (1997), but even Lyman-α pumping becomes significant ($y > 1$) only at $z \lesssim 15$ (in our fiducial model), when shock heating already dominates by a large margin.

An important conclusion of this demonstration is that the approximately linear decrease in the brightness temperature with frequency in the range $150\,\mathrm{MHz} \lesssim \nu \lesssim 200\,\mathrm{MHz}$ is robust; it is a manifestation of the reionization of the universe - the drop in the signal is simply due to neutral hydrogen atoms becoming ionized.

3.   Mean Signal

The first possible observable we consider is the mean (or global) emission in the redshifted 21 cm line, averaged over the whole sky (as we explain below, in practice this means signals on scales above about 2 degrees).
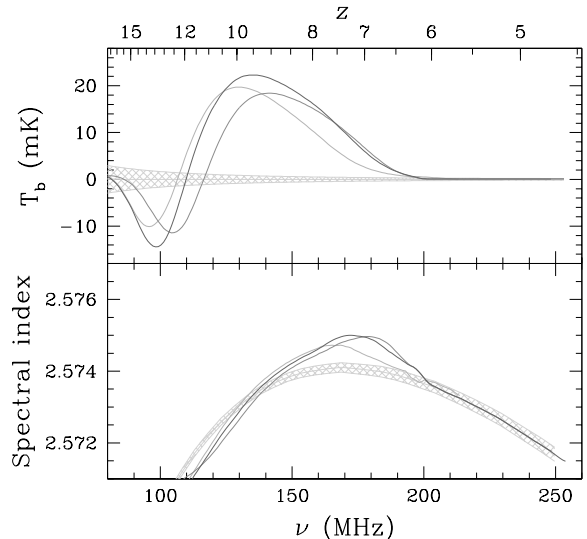

Fig. 3.— Top panel: The mean (over the whole sky) excess brightness temperature as a function of frequency and redshift for simulation sets A (dark gray), B (medium gray), and C (light gray). The thickness of the lightest gray (horizontal) band shows the $\pm 5\sigma$ sensitivity limit for a 10-day integration with a 5 MHz bandwidth ($1\sigma = 0.1\,\mathrm{mK}$ at 150 MHz independent of the telescope size; see Shaver et al. 1999). We omit this limit in subsequent figures as it is so small. Bottom panel: Spectral index vs frequency for the three simulation sets with the galactic and extragalactic foreground included according to the model of Shaver et al. (1999). The lightest gray hatched band gives the $\pm 5\sigma$ sensitivity limit for 10 days of integration (see explanation in the text).

Figure 3 shows the mean excess brightness temperature as a function of frequency and redshift for the simulation sets A, B, and C, and the resulting change in the spectral index of the total emission (including the galactic and extra-galactic foreground). We used the model of Shaver et al. (1999) for the foreground component in the bottom panel of Fig. 3, which includes galactic thermal and non-thermal components, and extragalactic sources. We also show an estimate of the $\pm 5\sigma$ sensitivity limit for a 10-day integration time for a system temperature of 200 K (this limit is independent of telescope size), as given by equation (6) of Shaver et al. (1999).

The three theoretical curves in Fig. 3 show the possible spread in the predicted values when variations in cosmological parameters are allowed. The predicted variation in the spectral index is well above the sensitivity limits, and it is clear from both panels of Fig. 3 that sensitivity is not an issue in the detection of the H I signal. The issue is how well the signal can be distinguished from the varying foreground spectrum. (Calibration and radio interference are of course also major concerns, and we address the reader to Shaver et al. (1999) for a discussion of these technical matters.)

The difference in the spectral index between the prediction for the total signal (the cosmological signal plus foreground emission) is easily distinguishable from the foreground, but, of course, we do not have the privilege to observe the foreground signal alone. The foreground must be estimated and the cosmological signal extracted from one observed total signal. Shaver et al. (1999) considered various possible strategies, including interpolations and extrapolations from frequencies outside the expected signal range, and a "trend analysis" approach. In the present analysis we have tried fitting a low order polynomial to the total signal as a surrogate for measuring the smooth foreground signal, but we found the results to be marginal and strongly dependent on the frequency range used to make a polynomial fit (this range is also seriously constrained by the presence of FM bands below 108 MHz and TV bands above 174 MHz). We have also tried to use a power spectrum analysis of the spectral index to pick up high frequency variations, and found this approach to be relatively insensitive to the presence of the cosmological signal. Thus, we conclude that the mean signal is not easily separable from the smooth foreground, although sophisticated statistical approaches might yield more success.

As mentioned above, all simulations are normalized to reproduce the observed mean transmitted flux in the spectra of SDSS quasars at $z \sim 6$. This observational constraint is a great advantage, as it leaves relatively small freedom in the possible variation of the excess brightness temperature. However, there is uncertainty about the beginning and duration of the pre-reionization era, which has been highlighted by the recent WMAP results.

The first results from the WMAP experiment indicated a high value ($\tau \sim 0.17$) of the optical
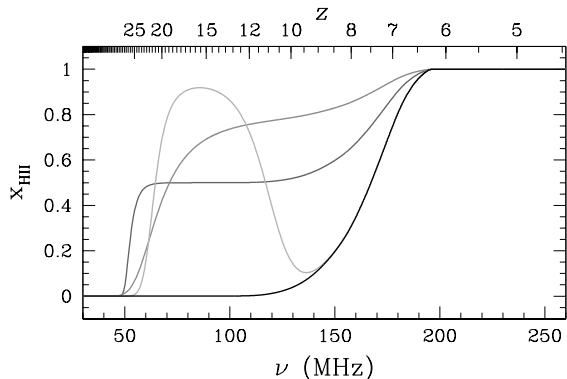

Fig. 4.— Ionization histories (volume averaged ionized fraction as a function of redshift) for our fiducial model A (black line; $\tau = 0.06$) and three arbitrary models with $\tau = 0.2$ (grey lines).

depth to Thompson scattering (Kogut et al. 2003). While these results have not been confirmed by a more comprehensive analysis of the combined WMAP and SDSS data (Tegmark et al. 2004), the possibility of a prolonged pre-reionization era remains an interesting one (Madau, Ferrara, & Rees 2001; Oh et al. 2001; Oh 2001; Venkatesan, Giroux, & Shull 2001). In order to investigate the possible effect a prolonged pre-reionization era might have on the observations of the 21 cm emission, we have constructed three reionization models that all produce an optical depth to Thompson scattering of $\tau = 0.2$ - about 1σ above the best-estimate value of Tegmark et al. (2004). These ionization histories are shown in Figure 4 together with out fiducial model from the simulation set A.

It is important to underline that these ionization histories are obtained arbitrarily, and are not results of simulations - in fact, the nature of ionizing sources that can produce such histories is not known. More than that, the light grey curve, which is designed to mimic "double reionization" (Cen 2003), is, in fact, unphysical, as low density regions in the universe will not be able to recombine between redshifts 12 and 7. Hence, these ionization histories only serve to illustrate the sensitivity of the redshifted 21 cm H I measurement as a tool for discriminating various ionization histories. The respective predictions for the mean signal are shown in Figure 5. As one can see, the 21 cm measurement may be used to constrain ionization
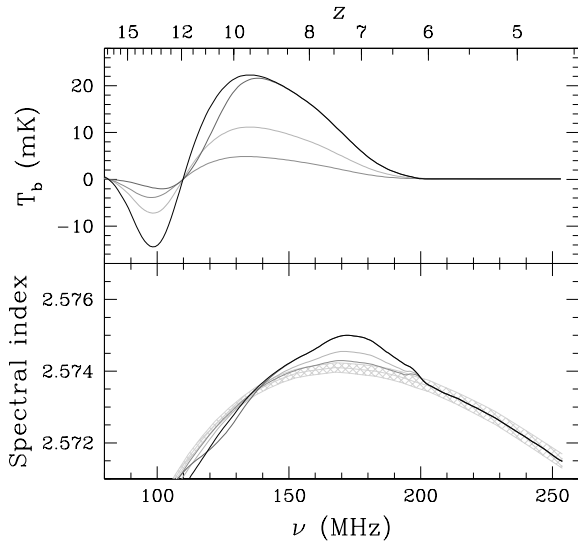
Fig. 5.— The same as Fig. 3, but for the ionization histories from Fig. 4.

histories in which the universe remains partially ionized for a prolonged period of time, but is not sensitive to the models in which the universe was reionized twice. However, as we have mentioned above, such models are not very plausible.

4. Fluctuations in $21\,\mathrm{cm}$ Emission

The $21\,\mathrm{cm}$ signal is not, of course, completely uniform over the sky: there are several sources of fluctuations in the $21\,\mathrm{cm}$ signal at high redshift.

At the redshifts of interest ($z \sim 10$), a given comoving size Δx corresponds to the angular size

$$\Delta\theta = 0'.6 C_z \frac{\Delta x}{h^{-1}\,\mathrm{Mpc}}$$

and the range of frequencies in the redshifted $21\,\mathrm{cm}$ line

$$\Delta\nu = 0.1\,\mathrm{MHz} D_z \frac{\Delta x}{h^{-1}\,\mathrm{Mpc}},$$

where C_z and D_z are weak functions of z in the redshift interval $6 < z < 10$. For $\Omega_{m,0} = 0.35$ at $z = 9$, $C_z = 0.938$ and $D_z = 0.894$. Thus, any realistic observation with $\Delta\nu \gtrsim 1\,\mathrm{MHz}$ and $\Delta\theta \gtrsim 1'$ will probe the linear regime at $z \sim 7-12$ with $\Delta x \gtrsim 2h^{-1}\,\mathrm{Mpc}$.

The linear large-scale density fluctuations are the subject of this paper. As mentioned above, another possible source of fluctuations in the high redshift $21\,\mathrm{cm}$ emission are H II regions created by bright quasars well before the moment of reionization (Madau et al. 1997; Tozzi et al. 2000). Such H II regions, if big enough, could be prominent features scattered sparsely over the sky. However, the simulations presented in this paper do not encompass sufficiently large computational volumes to include luminous quasars. Models that include a representative sample of bright quasars require a different computational approach, and will be the subject of a future paper.

Fluctuations can also be caused by variations in the quantity $q = 1 - T_{\mathrm{CMB}}/T_S$, where T_S is the gas spin temperature. However, the simulations that we use in this paper suggest that such variations are negligible compared to the density variations.

Given the power spectrum of density fluctuations $P(k)$ (hereafter we assume that the gas follows the dark matter on large scales), the rms density fluctuation as a function of the angular resolution $\Delta\theta$ and the frequency bandwidth $\Delta\nu$ is given by the following equation:

$$\delta_{\mathrm{RMS}}^2 = \frac{1}{(2\pi)^3} \int\limits_{-\infty}^{\infty} dk_\parallel \int d^2 k_\perp P(k)\, e^{-k_\parallel^2 R_\parallel^2 - \vec{k}_\perp^2 R_\perp^2},$$

$$(2)$$

where $k_\parallel$ is the wavenumber along the line-of-sight (the frequency dimension), $\vec{k}_\perp$ is the wavevector in the plane of the sky (two angular dimensions), $k \equiv \sqrt{k_\parallel^2 + \vec{k}_\perp^2}$, and

$$R_\parallel = 1h^{-1}\,\mathrm{Mpc}\frac{\Delta\nu}{2.35 \times 0.1\,\mathrm{MHz} D_z}$$

and

$$R_\perp = 1h^{-1}\,\mathrm{Mpc}\frac{\Delta\theta}{2.35 \times 0'.6 C_z},$$

and the factor $2.35 = 2\sqrt{2\log 2}$ comes from the conversion from the FWHM to the gaussian dispersion.

As an example, Figure 6 shows linear fluctuations in a $20^o \times 20^o$ region of the sky. Because the fluctuations are gaussian, there are no distinct features in the image, and separating this signal from the random fluctuations in the foregrounds is a non-trivial task. A big enough quasar will create
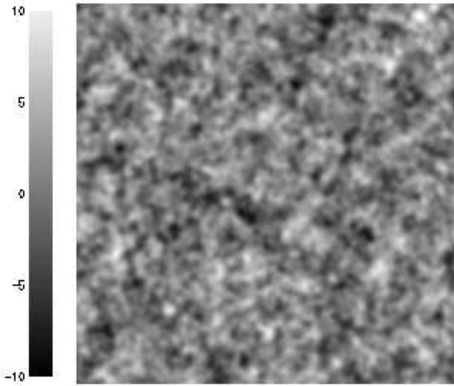
Fig. 6.— A $20^o \times 20^o$ image of fluctuations in the excess brightness temperature of the redshifted 21 cm line at $z = 9$ for our fiducial model (with $4'$ resolution and 1 MHz bandwidth). The color-bar on the left shows the scale in mK.

Fig. 7.— The excess brightness temperature (top) and its rms fluctuation (bottom) measured in a beam of $4'$ FWHM with 1 MHz bandwidth.

an H II region around itself, and will form a significant structure in the fluctuation map (Madau et al. 1997) - as mentioned above, this effect will be considered in a follow-up paper.

A complimentary view of the fluctuations in the redshifted 21 cm emission is provided in Figure 7, which shows the excess brightness temperature and its rms fluctuations for our three simulation sets as a function of frequency. The level of rms fluctuations on the scale we consider is only about 10% of the mean signal.

In order to determine whether the fluctuations are potentially observable, they have to be compared with the possible fluctuations in the foreground (galactic and extragalactic) emission.

4.1. Angular Fluctuations

As has been discussed by Di Matteo et al. (2002), angular fluctuations due to extragalactic radio sources are significantly larger than those from the pre-reionization era. In order to estimate the contribution of the extragalactic sources, Di Matteo et al. (2002) adopted a model for differential source counts at 150 MHz at low flux density levels, $N(S) \approx 700\,\mathrm{sr}^{-1}\,\mathrm{mJy}^{-1}(S/1\,\mathrm{mJy})^{-1.75}$, and a model for the source correlation function, $w(\theta) \approx (\theta/\theta_0)^{-0.85}$ with $\theta_0 = 4'$. While the indexes of the power-laws adopted by Di Matteo et al. (2002) agree with other studies, there exist surprising differences in the values of the am-
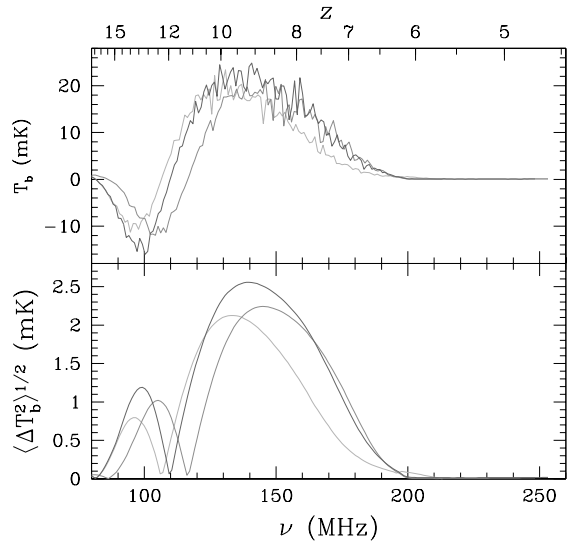
plitudes they adopted. For example, Hopkins et al. (1998) give the source number counts as $N(S) \approx 10\,\mathrm{sr}^{-1}\,\mathrm{mJy}^{-1}(S/1\,\mathrm{mJy})^{-1.75}$ at 1.4 GHz. Assuming that no new source population is present at 150 MHz that is not observed at 1.4 GHz, and that the source spectral index between 150 MHz and 1.4 GHz is about -0.75, the source flux density of 1 mJy at 1.4 GHz translates into 5.4 mJy at 150 MHz, which gives the source number counts at 150 MHz at $S = 1\,\mathrm{mJy}$ of about $200\,\mathrm{sr}^{-1}\,\mathrm{mJy}^{-1}$, a factor of 3.5 below the value adopted by Di Matteo et al. (2002). In addition, both FIRST and NVSS measurements of the extragalactic radio source correlation function give the functional form adopted by Di Matteo et al. (2002) but with $\theta_0 \approx 1'$ (Blake & Wall, 2002). The latter applies for sources brighter than a few mJy at 1.4 GHz - significantly brighter than sources considered by Di Matteo et al. (2002) - but it is difficult to imagine that faint sources are clustered more strongly than the bright ones. The total effect of these corrections would be to reduce the Di Matteo et al. (2002) estimate of the foreground fluctuations by a factor of 11.

On the other hand, Di Matteo et al. (2002), as one of their cases, showed their estimate when all sources above 1μ Jy have been removed from
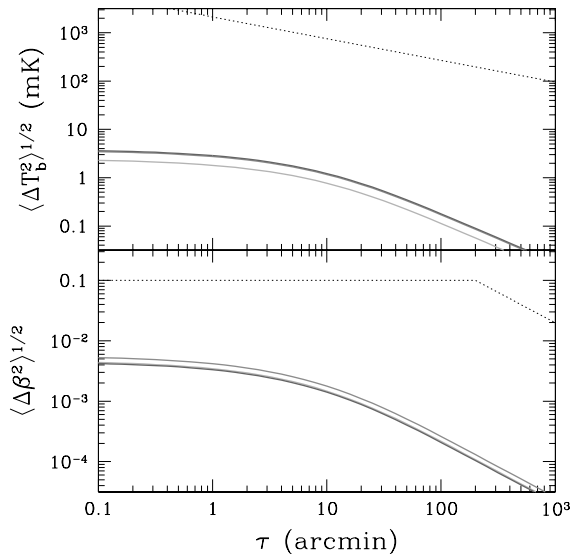
Fig. 8.— The rms excess brightness temperature fluctuations in 1 MHz bandwidth at $z = 8.5$ (top) and the rms *angular* fluctuation in the spectral index β (bottom) as a function of the angular scale. The dotted lines show the foreground contaminations: fluctuations due to residual point sources after all sources above 1μ Jy have been removed (top; Di Matteo et al. 2002) and variations in the spectral index of the galactic synchrotron emission (bottom; Banday & Wolfendale 1991). See the discussion in text for full explanation.

the data (thick black line in Fig. 1 of Di Matteo et al. 2002), which is, probably, an overly optimistic assumption. If we conservatively assume that only sources above 1 mJy can be effectively removed from the data or adequately modeled in the data analysis, then the estimate of angular fluctuations from the extragalactic radio sources would be a factor of 10 higher - but that is almost exactly compensated by the factor of 11 by which Di Matteo et al. (2002) overestimated the clustering signal of extragalactic point sources. Therefore, for the rest of this paper, we adopt the thick solid line from Fig. 1 of Di Matteo et al. (2002) as a reasonable estimate for the angular fluctuations in the 21 cm signal due to the clustering of extragalactic radio sources.

As can be seen from the top panel of Figure 8, our results fully agree with the conclusions of Di

Matteo et al. (2002): the contamination by the extragalactic source population makes it highly unlikely that the predicted levels of the 21 cm fluctuation signal from the pre-reionization era can be reached.

Not only the extragalactic radio sources, but also the even stronger galactic foreground emission will produce substantial angular fluctuations in the emission over the sky. Such fluctuations may extend down to quite small angular scales, and can only add to the already dominant fluctuations from the extragalactic source population. The small contribution from galactic thermal emission will certainly add to the fluctuation signal - it may be similar to the structure in the galactic infrared cirrus. There may in addition be other contributors to the foreground angular fluctuation signal, such as the extended radio emission from clusters of galaxies. Thus, in view of the overwhelming foreground contamination, it seems highly unlikely that the angular fluctuations in the redshifted H I signal will by themselves be useful in studying the pre-reionization era.

Can one possibly use frequency information to help separate the angular fluctuations in the HI signal from the foreground fluctuations, as the spectra of the foregrounds are expected to be smooth, with only gradual changes in spectral index? In order to investigate this possibility, we computed the angular variation in the spectral index on the sky as the difference between two images taken 5 MHz apart. The bottom panel of Fig. 8 shows the rms spectral index fluctuations as a function of angular scale at 150 MHz ($z = 8.5$). Unfortunately, spatial variations in the spectral index of the galactic synchrotron emission make this approach difficult if not impossible. Banday & Wolfendale (1991) estimate variations of the order of 0.1 on angular scales of $3^o.5$. While their estimate applies to the frequency range from 400 to 800 MHz, it is reasonable to assume that similar variations exist at frequencies around 150 MHz. The dotted line in the bottom panel of Fig. 8 shows a simple toy model for the variation in the spectral index of the galactic synchrotron emission: we take Banday & Wolfendale's (1991) value of 0.1 at $3^o.5$, and then assume that fluctuations are uncorrelated on larger scales and remain fixed on smaller scales. This lower limit is overly conservative, since Banday & Wolfendale (1991) indicate that

fluctuations in the spectral index are correlated on angular scales above 3°, and on smaller angular scales fluctuations are expected to be higher because the angular scale of 3° does not correspond to any particular physical scale.

There may be other more sophisticated techniques that can be employed in analyzing the observed data cube. However, on the basis of present knowledge, we conclude that the angular fluctuations will be extremely difficult if not impossible to utilize in measuring and studying the H I signal.

4.2. Fluctuations in the Frequency Domain

If the angular fluctuations are not observable, one may still hope to use the fact that all known radio foregrounds are expected to be relatively smooth functions of frequency, and rely on the frequency information alone to separate the cosmological signal. For the cosmological signal the frequency direction is just another spatial dimension, and so the cosmological signal should fluctuate in frequency space very much as it fluctuates over the sky. By contrast, the foreground contamination is totally different in the angular and frequency dimensions: the foreground angular signal has all the structure of a distribution of point sources over the sky, whereas the foreground frequency signal is just a sum of smooth spectra, hence itself a smooth function, against which the relatively sharp cosmological fluctuations (in frequency) should stand out clearly. This approach may in fact be by far the best one to studying the reionization H I signal. Other authors (e.g. Di Matteo et al. 2002) have also recognized this possibility; here we quantify it and show the dependence on observational parameters such as beam size and bandwidth.

Figure 9 shows the H I fluctuations superimposed on the combined spectrum of the galactic and extragalactic foregrounds (spectral index is used here in order to be able to show both the H I and foreground signals on a single plot). The difference between the frequency structure of the H I signal and the foregrounds is immediately obvious, and it is clear that one may study the former with not too much complication from the latter. Thus, it appears that the best strategy for measuring the reionization signal may be to forsake any attempt to measure angular fluctuations
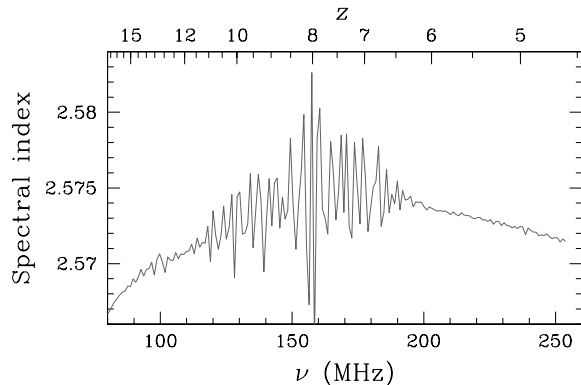

Fig. 9.— The spectral index of the total signal (H I signal plus the foregrounds) in a beam of $4'$ FWHM with a $1\,\mathrm{MHz}$ bandwidth.

and concentrate on frequency fluctuations alone. Thanks to the relative spectral smoothness of the foreground emissions, this is almost certainly the best approach to detect and study the reionization H I signal. (Note that we assume here that the beamsize is independent of frequency; the effect of a frequency-dependent beam is considered below.)

The excess brightness temperature fluctuations (with the mean signal subtracted) are shown in Figure 10 for several values of the beam size and bandwidth. As can be seen from the figures, the frequency fluctuations are a strong function of the beam size (which we specify at $150\,\mathrm{MHz}$) and the bandwidth, but for a large range of beam sizes and bandwidths they are well above the sensitivity limits (for example, for a $4'$ beam and $1\,\mathrm{MHz}$ bandwidth the signal-to-noise ratio at $150\,\mathrm{MHz}$ is about 22 for a 40-day integration).

The fluctuations in the frequency domain depend on the bandwidth. Is there an optimal range for the value of the bandwidth? Obviously, fluctuations are smaller on the larger scales. However, the sensitivity is also higher for larger bandwidths. It turns out that these two effects almost cancel each other: Figure 11 shows that for bandwidths in excess of about $1\,\mathrm{MHz}$, the signal-to-noise ratio is essentially constant, so the exact value of the bandwidth is probably not that important.

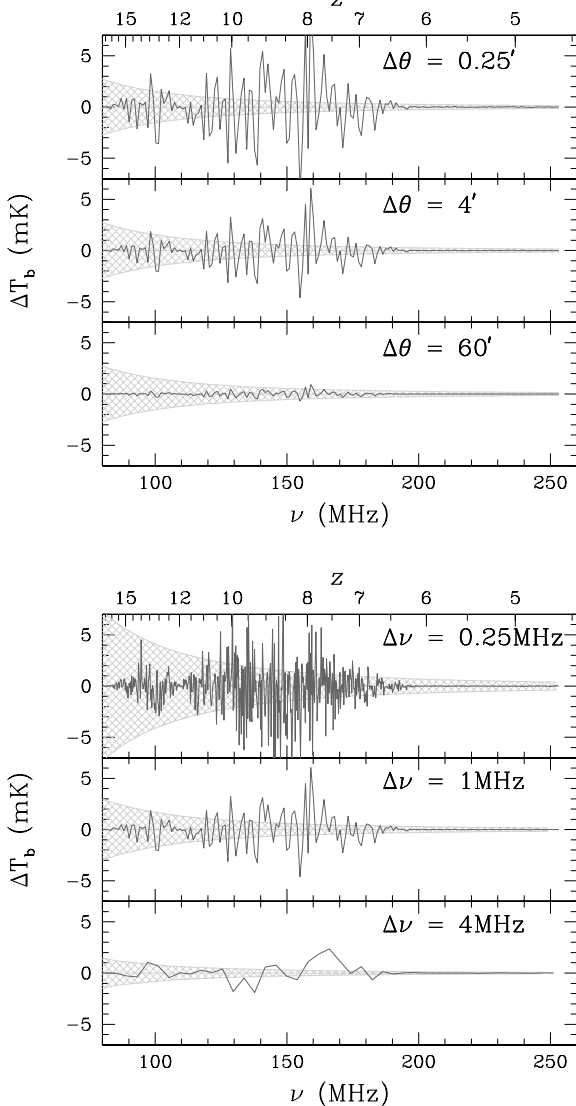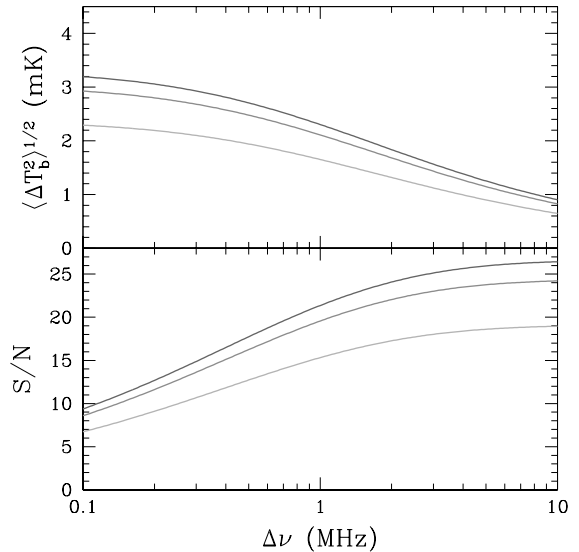In order to illustrate the measurability of the fluctuation signal in the frequency domain, we

10

Fig. 11.— The rms excess brightness temperature fluctuations on angular scales of 4′ at $z = 8.5$ as a function of bandwidth (top) and the respective signal-to-noise ratio (bottom) for a 40-day integration.

Fig. 10.— (a) The excess brightness temperature fluctuations (with the mean signal substructed) for an observation with a fixed bandwidth of 1 MHz and varied beam size at 150 MHz (assuming an appropriate telescope size). The hatched regions give ±5σ sensitivity limit for a 40-day integration time for the foreground model of Shaver et al. (1999). (b) The same as (a) but for a fixed beam size of 4′ at 150 MHz and varied bandwidth.

present in Figure 12 contours of fixed signal-to-noise ratio for various beam sizes, bandwidths, and integration times, as a guide for developing an observational strategy. Since our fiducial model is based only on known physical processes and does not include an extended period of reionization, it can serve as an upper limit for the expected signal (except for the occasional presence of a luminous QSO in the beam). Thus, the signal-to-noise ratio of a real experiment may be smaller, but generally will not be larger, than the one shown in Fig. 12.

The top panel of Fig. 12 also shows what angular and frequency scales one needs in order to measure the mean signal: S/N=3 for the fluctuations essentially means that fluctuations are unobservable, so different patches of the sky larger than about 2 degrees will have the same signal within the sensitivity limit (for a 40-day integration).

The feasibility of measuring the frequency signal will, of course, critically depend on the ability to calibrate different frequency bands to within a fraction of a mK. Such an observation may be done, for example, by beam switching between the target area on the sky and a strong nearby extra-
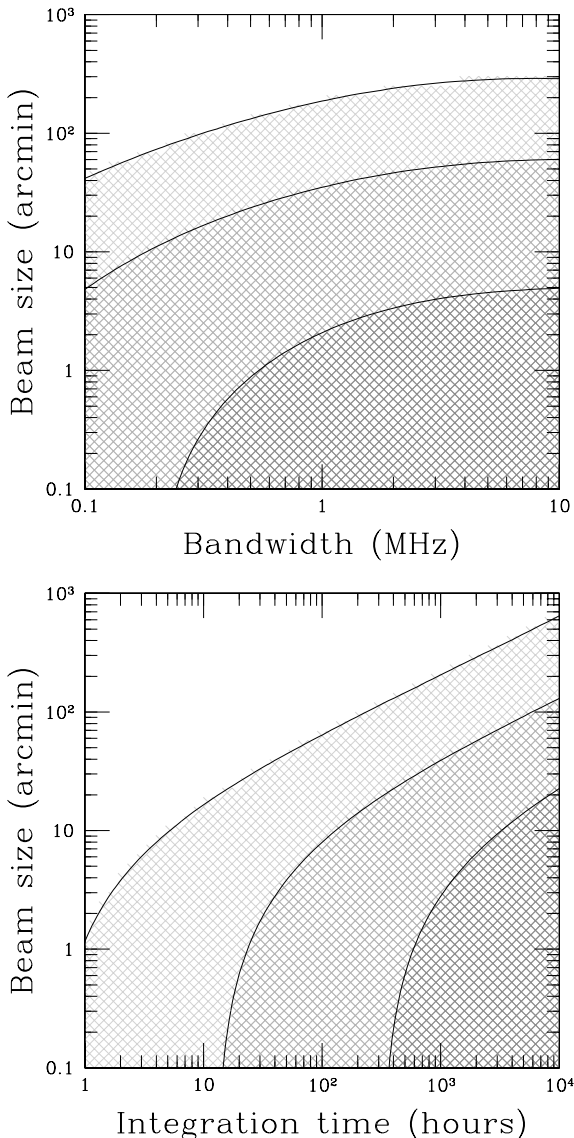
Fig. 12.— Contours of signal-to-noise ratio in the fiducial model for the rms excess brightness temperature fluctuation at $150\,\mathrm{MHz}$ ($z = 8.5$) and assuming the system temperature of $200\,\mathrm{K}$ as a function of bandwidth and *filled aperture* beam size for the integration time of 40 days (a) and as a function of integration time and the beam size for $1\,\mathrm{MHz}$ bandwidth (b). Shown are contours of S/N=1 (light gray area), S/N=5 (medium gray area), and S/N=25 (dark gray area). The signal-to-noise will be respectively lower for extended reionization models.

galactic radio source, whose spectrum is expected to be very smooth on $1\,\mathrm{MHz}$ frequency scales. This approach would be difficult or impossible for the detection of the mean (all-sky) signal, as discussed by Shaver et al. (1999), because the frequency dependence of the mean H I signal is relatively smooth, but in the case of the sharp frequency variations of the fluctuation signal it should become possible. This could be a great advantage because relative measurements are far easier to make than absolute measurements.

There will be some natural narrow-band contaminants of the frequency signal, such as galactic radio recombination lines. However these show up at well-known frequencies (separated by typically $1 - 2\,\mathrm{MHz}$ in this frequency range), and they are narrow, so they can be removed from the data. A major potential contaminant, of course, is man-made RFI. However, it is variable and generally very narrow-band; techniques are being developed to identify and excise such contamination. How completely such contamination can be removed remains to be determined, however. To the extent that spectral contaminants show up predominantly in emission, whereas the fluctuations in Fig. 10 go both ways, in emission and in absorption relative to the smooth foreground, it may be possible to use these properties to help identify and characterize the signal. Furthermore, as the cosmological parameters to be extracted from the gaussian H I signal are the same in all directions of the sky, observations in different directions should ultimately give the same results.

In addition to the contaminants mentioned above, there is another effect that can potentially obscure the cosmological H I signal: the leakage of the angular fluctuations into the frequency domain due to the frequency-dependent beam size (Oh & Mack 2004; Di Matteo et al. 2002). In the simplest case of a single filled aperture, it is inversely proportional to the frequency of observations. In order to see fluctuations in the cosmological H I signal, one has to observe over a range of frequencies, and because observations at different frequencies have different beam sizes, they sample different regions of the sky. The angular fluctuations between the observed brightness temperature in these different regions appear as fluctuations in the frequency domain.

It is straightforward to estimate this effect. Us-

12

ing equation (4) of Di Matteo et al. (2002), we approximate the power spectrum of fluctuations in a beam with a gaussian width σ as

$$C_l = A^2 l^{\beta-2} e^{-l^2\sigma^2/2}, \qquad (3)$$

where C_l is the total power in a spherical multipole l, A is the amplitude of fluctuations at $l = 1$, and $\beta \approx 0.85$ is the power-law index of the fluctuation angular correlation function.

Let $T(\vec{\Omega}, \sigma)$ be a temperature fluctuation in a beam with a gaussian width σ in the direction $\vec{\Omega}$ on the sky. Two observations in the direction $\vec{\Omega}$ spaced in frequency by $\Delta\nu$ would see the rms difference in the brightness temperature:

$$\delta T_{\mathrm{RMS}} \equiv \Delta\sigma \left\langle \left(\frac{dT(\vec{\Omega}, \sigma)}{d\sigma} \right)^2 \right\rangle^{1/2} =$$

$$\sqrt{\beta(\beta+1)} \frac{\Delta\sigma}{\sigma} T_{\mathrm{RMS}}, \qquad (4)$$

where T_{RMS} is the rms angular temperature fluctuation in the beam σ, and $\Delta\sigma/\sigma = \Delta\nu/\nu$. For a beam with FWHM of $4'$ this estimate gives a value of about $6\,\mathrm{mK}$ at $150\,\mathrm{MHz}$ for $T_{\mathrm{RMS}} = 1\,\mathrm{K}$. This fact was noted by Di Matteo et al. (2002) and Oh & Mack (2004) as a severe obstacle for measuring cosmological fluctuations in the frequency domain. However, these previous works missed the fact that the leaked angular fluctuations are strongly correlated. Let us consider three beams A, B, and C spaced by $\Delta\nu$ in frequency, with beam sizes θ_A, θ_B, and θ_C. The signal in beam A will differ from the signal in beam B by some amount due to sources located within the ring on the sky with a radius of $(\theta_A + \theta_B)/2$ and the width of $\theta_B - \theta_A$. Analogously, the signal in beam B will differ from the signal in beam C due to sources located within a ring from θ_B to θ_C. But because these two rings are adjacent to each other, sources within the ring $\theta_B - \theta_A$ are strongly correlated with the sources within the ring $\theta_C - \theta_A$, so that the increase or decrease in the total signal in beams B and C due to fluctuations will be a relatively smooth function of frequency as well, and the frequency fluctuations from the leakage signal will be much smaller. Namely, given a temperature difference T_{BA} between beams B and A and the temperature difference T_{CB} between beams C and
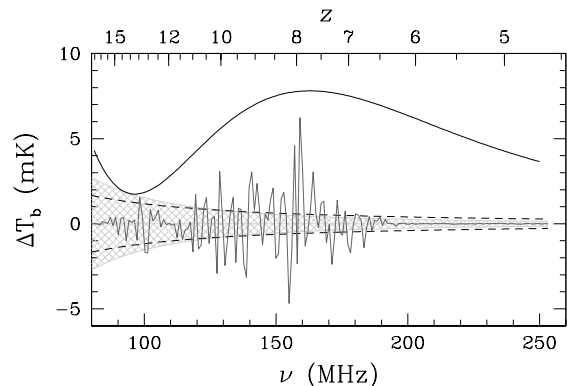

Fig. 13.— The excess brightness temperature fluctuations (with the mean signal substructed) for an observation with a fixed bandwidth of $1\,\mathrm{MHz}$ and a *frequency-dependent* beam size of $4'$ at $150\,\mathrm{MHz}$ (similar to the middle panel of Fig. 10 but with the frequency dependence of the beam size taken into account) together with a realization of a frequency fluctuation due to leakage of angular fluctuations into the frequency domain (solid black line). The hatched regions give $\pm 5\sigma$ sensitivity limit for a 40-day integration time for the foreground model of Shaver et al. (1999), and the black dashed lines show characteristic $\pm 5\sigma$ errors due to angular fluctuation leakage (eq. [5]).

B, the rms difference between these two temperatures $\Delta T_{\mathrm{RMS}} \equiv \left\langle (T_{CB} - T_{BA})^2 \right\rangle^{1/2}$ is

$$\Delta T_{\mathrm{RMS}} = \Delta\sigma \left\langle \left(\frac{d\delta T(\vec{\Omega}, \sigma)}{d\sigma} \right)^2 \right\rangle^{1/2} =$$

$$\sqrt{2\beta(\beta^2 + 4\beta + 7)} \left(\frac{\Delta\sigma}{\sigma} \right)^2 T_{\mathrm{RMS}}, \qquad (5)$$

another factor of $\Delta\nu/\nu \approx 1/150$ smaller.

In order to illustrate this fact further, we have simulated the leakage effect by constructing a sample of the sky with gaussian fluctuations[2] having a power-law power spectrum, as given by equation (4) of Di Matteo et al. (2002). We then computed the temperature within the gaussian beam of variable size $\theta = 4'(\nu/150\,\mathrm{MHz})$ for ν ranging from

---

[2] The assumption of gaussianity is a good one as long as the number of point sources within the beam is large, which is the case for the values of the beam size considered here.

80 to 250 MHz in increments of 1 MHz (the bandwidth used in the middle panel of Fig. 10), centered at a random point on the simulated region of the sky. One realization of the leakage signal within the beam is shown in Figure 13. The black solid line gives the leaking angular fluctuation δT, and the two black dashed lines show the $\pm 5\sigma$ levels of contamination of the cosmological H I signal expected in this case ($5 \times \Delta T_{\mathrm{RMS}}$). As one can see, the contamination is comparable to the observational noise for a 40-day integration, so it becomes the dominant component of noise for longer integration times. Thus, it will not be useful to use integration times well in excess of 40 days on a given field.

Figure 14 illustrates possible observational choices when the angular fluctuation leakage is included as a source of noise. The top panel of Fig. 14 shows contours of signal-to-noise ratio with only leakage noise included - these contours scale in inverse proportion to the amplitude of angular fluctuation on the beam scale. The bottom panel includes both the observational noise and the leakage noise. While the bottom panel is the most complete representation of possible observational signal-to-noise ratio for our model, the contours on the bottom panel depend on both the integration time and the amplitude of angular fluctuations on the beam scale and scale non-trivially when these quantities are changed. Therefore, while this panel can be used as an illustration of possibilities, it is only applicable for the values of observational or theoretical parameters adopted in this paper.

Other sources of angular fluctuations that might produce leakage in the frequency domain are the galactic synchrotron and thermal emission. If the galactic emission is not structured more strongly on scales of tens of arcminutes than the extragalactic point source contamination, then it will not present a significant obstacle to measuring the cosmological H I signal, but this question requires further investigation, including more detailed observations of the galactic emission.

There are various ways in which the leakage of angular fluctuations could be minimized. The most important would obviously be to observe with the same beam size at all frequencies. This could best be approximated with the use of scaled arrays especially designed to control the synthe-
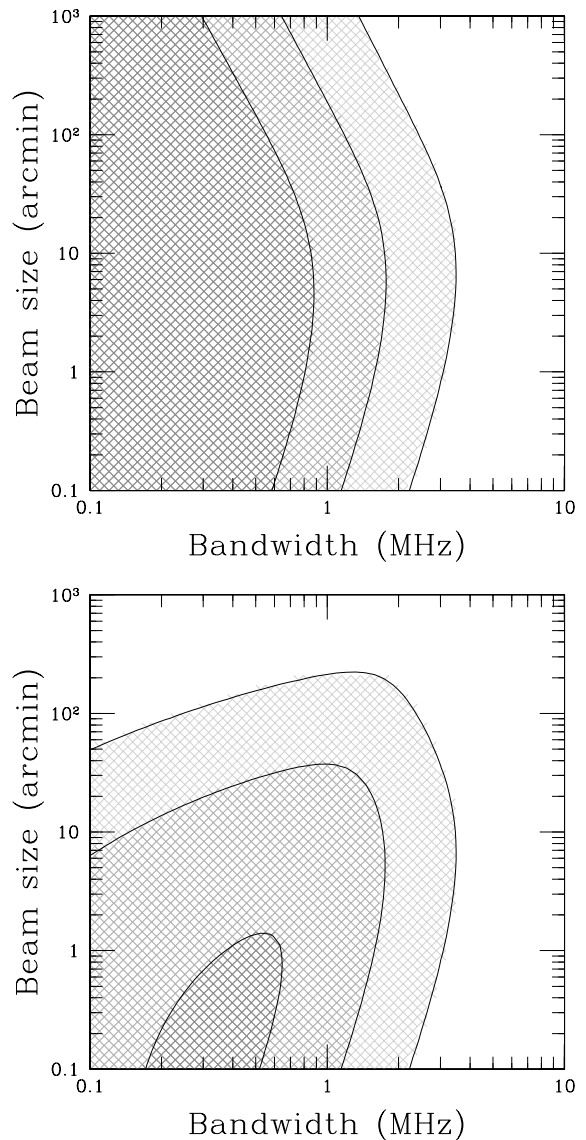

Fig. 14.— (a) Contours of signal-to-noise ratio in the fiducial model for the rms excess brightness temperature fluctuation at 150 MHz ($z = 8.5$) and assuming a system temperature of 200 K as a function of bandwidth and *filled aperture* beam size with the noise entirely due to angular fluctuation leakage (eq. [5]). Shown are contours of S/N=1 (light gray area), S/N=5 (medium gray area), and S/N=25 (dark gray area). (b) Contours of signal-to-noise ratio for the same observational parameters, with both observational noise (for a 40-day integration) and the leakage noise, included in quadrature.

sized beam and sidelobes. For filled-aperture telescopes, frequency-dependent illumination of the reflector would be required, at least over a limited frequency range, but this would then utilize only a fraction of the total aperture, and would undoubtedly be a major technical challenge. In any case it would clearly be advantageous to observe in directions of the sky where the foreground contamination is lowest: regions of low extragalactic source density and fluctuations, and regions of high galactic latitude where the galactic emission is weakest and smoothest.

5. Conclusions

The challenge in observing the redshifted 21 cm line of neutral hydrogen from the pre-reionization era is not that it is weak, but rather that it is hidden behind strong foreground emission (both galactic and extragalactic). Our results confirm the conclusions of other authors that detection of the angular fluctuations on the sky will be extremely difficult or impossible because of the huge contamination from fluctuations in the foreground emissions.

Better opportunities are provided by the fact that the radio foregrounds are slowly varying as a function of frequency. This generic feature might make it feasible (although very challenging) to detect the overall mean signal from the pre-reionization era. This signal would be the true average over the whole sky, which in practice means a signal on scales larger than about two degrees - the signal on these scales is expected to be the same in all directions on the sky.

However, by far the best opportunity to measure the cosmological signal (again thanks to the spectral smoothness of the foregrounds) is offered by its frequency structure. The large-scale density fluctuations in a single beam are uncorrelated on frequency scales above about $0.2 - 0.3\,\mathrm{MHz}$, so that the excess brightness temperature varies by about $2 - 3\,\mathrm{mK}$ and the local spectral index of the radio signal varies by about 0.4% on scales of the order of $1\,\mathrm{MHz}$. These sharp variations should not be difficult to separate from the smoothly varying foreground signal.

Thus, the frequency fluctuation signal stands out in comparison with the other two possibilities (mean signal and angular fluctuations). While the

observability of the latter two depends critically on confusion with foregrounds, the former may be largely just a matter of sensitivity. Frequency calibration, contamination by spectral lines or leakage of angular fluctuations, and RFI may all be manageable problems. Using our simulations we have shown that it may then be possible to detect the H I signal from the pre-reionization era even at moderate angular resolution ($\sim 10 - 20$ arcmin), corresponding to filled apertures of a few hundred meters diameter.

REFERENCES

Banday, A. J., & Wolfendale, A. W. 1991, MNRAS, 248, 705

Blake, C., & Wall, J. 2002, MNRAS, 337, 993

Cen, R. 2003, ApJ, 597, L13

Chen, X., & Miralda-Escudé, J. 2004, ApJ, in press (astro-ph/0303395)

Ciardi, B.; Ferrara, A.; White, S. D. M. 2003, MNRAS, 344, L7

Ciardi, B., Madau, P. 2003, ApJ, 596, 1

Ciardi, B.; Stoehr, F.; White, S. D. M. 2003, MNRAS, 343, 1101

Cress, C. M., Helfand, D. J., Becker, R. H., Gregg, M. D., & White, R. L. 1996, ApJ, 473, 7

Di Matteo, T., Perna, R., Abel, T., & Rees, M. J. 2002, ApJ, 564, 676

Fan, X., at al. 2003, AJ, 125, 1649

Furlanetto, S. R., Sokasian, A., & Hernquist, L. 2004, MNRAS, in press (astro-ph/0305065)

Gnedin, N. Y. 2000, ApJ, 535, 530

Gnedin, N. Y., & Abel, T. 2001, NewA, 6, 437

Gnedin, N. Y., & Bertschinger, E. 1996, ApJ, 470, 115

Gnedin, N. Y., & Ostriker, J. P. 1997, ApJ, 486, 581

Hopkins, A. M., Mobasher, B., Gram, L., & Rowan-Robinson, M. 1998, MNRAS, 296, 839

Iliev, I. T., Shapiro, P. R., Ferrara, A., & Martel, H. 2002, ApJ, 572, L123

Iliev, I. T., Scannapieco, E., Martel, H., & Shapiro, P. R. 2003, MNRAS, 341, 81

Kogut, A., et al. 2003, ApJS, 148, 161

Madau, P., Ferrara, A., & Rees, M. J. 2001, ApJ, 555, 92

Madau, P., Meiksin, A., & Rees, M. J. 1997, ApJ, 475, 429

Oh, S. P. 2001, ApJ, 553, 499

Oh, P. S., & Mack, K. J. 2004, MNRAS, in press (astro-ph/0302099)

Oh, S. P., Nollett, K. M., Madau, P., & Wasserburg, G. J. 2001, ApJ, 562, L1

Ricotti, M., Gnedin, N. Y., & Shull, J. M. 2003, ApJ, 575, 49

Scott, D., & Rees, M. J. 1990, MNRAS, 247, 510

Shaver, P. A., Windhorst, R. A., Madau, P., & de Bruyn, A. G. 1999, A&A, 345, 380

Sokasian, A., Abel, T., Hernquist, L., & Springel, V. 2003, MNRAS, 344, 607

Spergel, D. N., et al. 2003, ApJS, 148, 175

Steidel, C. C., Adelberger, K. L., Ciavalisco, M., Dickinson, & M., Pettini, M. 1999, ApJ, 519, 1

Sunyaev, R. A., & Zel'dovich, Ya. B. 1972, A&, 20, 189

Tegmark, M., et al. 2004, ApJ, submitted (astro-ph/0310723)

Tozzi, P., Madau, P., Meiksin, A., & Rees, M. J. 2000, ApJ, 528, 597

Venkatesan, A., Giroux, M. L., & Shull, J. M. 2001, ApJ, 563, 1

White, M., & Bunn, E. F. 1995, ApJ, 450, 477

White, R. L., Becker, R. H., Fan, X., & Strauss, M. A. 2003, AJ, 126, 1

Zaldarriaga, M., Furlanetto, S. R., & Hernquist, L. 2004, ApJ, submitted (astro-ph/0311514)